3D printed ABS-MOF composite materials and their gas storage properties

Michael Bible[a], Makfir Sefa[b], James A. Fedchak[b], Julia Scherschligt[b], Zeeshan Ahmed[b]*, Matthew R. Hartings[a]*

[a]Department of Chemistry, American University, 4400 Massachusetts Ave., NW, Washington, DC 20016, USA

[b]Thermodynamic Metrology Group, Sensor Science Division, Physical Measurement Laboratory, National Institute of Standards and Technology, Gaithersburg, MD 20899, USA

Abstract:

Metal organic framework materials (MOFs) have been primarily recognized for their ability to promote selective storage of gas molecules. In their as-synthesized (powdered) form, MOFs are not easily processed for use in end-devices where their properties are to be exploited. We have produced composites in which either ZIF-8 or HKUST-1 have been incorporated into acrylonitrile butadiene styrene (ABS). These composites were then 3D printed using a conventional, commercially available 3D printer. Although many MOFs suffer from instability in humid environments, each of the MOF's in our study maintains its structure within the ABS composite even upon soaking in water. Moreover, the MOFs maintain their nitrogen adsorption capacities within the composites. Spectroscopic, thermophysical analysis, gas adsorption isotherms, and gas adsorption and desorption studies for ABS-ZIF-8 composites reveal an ideal system that behaves as a 9:1 linear combination of ABS and ZIF-8. The same analysis for ABS-HKUST-1, however, reveals a more complex system where the composite significantly reduced gas adsorption capacity at 77 K and slower adsorption and desorption profiles at room temperature. Our thermo-physical analysis indicates that these changes are likely due to the HKUST-1 altering the structural and, therefore, gas adsorption and diffusion properties of the ABS

by inducing stronger polymer-polymer interactions. Nonetheless, at room temperature the HKUST-1 composite displays a higher nitrogen adsorption capacity than the ZIF-8 composite. The retention of MOF gas adsorption properties within the composite is promising in that these materials can be optimized (MOF, polymer, and 3D printed geometry) for a number of applications including gas storage, filtering, sensing, and catalysis.

Introduction

3D printing technologies have steadily made their way into the laboratories of research chemists. The Cronin group has pioneered the use of 3D printers to create custom reactionware[1] and combined this with computer-controlled liquid handling to enable automated chemical synthesis.[2] Scientists with a more biomaterials slant to their research have been printing hydrogels and other soft materials that support mammalian cell growth and differentiation.[3-9] And, while most 3D printing methods rely on squeezing a thermoplastic or other thixotropic material through a nozzle, other scientists have developed a different additive manufacturing technique based on polymer chemistry. DeSimone and coworkers created a light-induced polymerization process for generating complex material geometries.[10]

Our approach to 3D printing is to imbue active chemical reactivity and functionality within the 3D printed material. That is, whereas most 3D printed objects are, necessarily, inert, we aim to 3D print materials that play an active role in supporting and facilitating chemical processes.[11] Our approach to generating these materials is to create a composite of a 3D printing matrix material with chemically reactive nanoparticles or microparticles. This approach is not unique to us. Others like Worsley and coworkers

have produced 3D printed graphene aerogels by printing a graphene composite material and thermally degrading its matrix.[12] We have focused on incorporating inorganic nanoparticles within standard 3D printing thermoplastics.[11] One of our goals is to create 3D printing filaments that can be used in standard, commercial thermoplastic printers that typically use either ABS or poly lactic acid (PLA). In our first trial of this approach, we incorporated nanoparticulate TiO_2 into ABS.[11] We found that the TiO_2 retained its ability to photocatalyze the degradation of organic compounds while in the 3D printed composite.

Applying this approach to other, chemically interesting particles, we have translated these techniques to the incorporation of MOFs into 3D printed polymers. MOFs have a repeating 3-dimensional structure whose coordination driven arrangement of metal ions and ligating organic molecules leads to the formation of repeated vacancies within the bulk material.[13-15] Development of novel methods that enable the use these geometries for gas storage (within the MOF vacancies) and chemical catalysis (at the structured metal sizes) is an active area of research.[13-16] The great potential of MOFs, however, is somewhat tempered by their lack of immediate processibility. During synthesis MOF particles precipitate as fine powders that do not easily lend themselves to being incorporated into larger devices or structures where they might be better utilized. Another shortcoming includes the instability of some MOFs in humid environments.[17, 18]

One approach to address these issues is to incorporate MOFs within a polymer matrix.[19-21] Of particular note, with respect to these efforts, has been the research of Cohen and coworkers. They have synthesized polymers, which are directly incorporated

into the MOF architecture.[22, 23] They have also made polymer-MOF composite films that show tolerance to functioning in humid environments.[17, 24]

We have extended this approach to incorporating MOFs within ABS, creating a filament for 3D printing, and printing different geometries using a commercially available 3D printer (Figure 1). We used two MOFs for this study, HKUST-1 and ZIF-8. We tested several physical properties of the composite materials as well as the stability of the MOFs within the composite when exposed to water. We also tested the nitrogen adsorption properties of our composite materials by measuring isotherms at 77 K and adsorption-desorption kinetics at room temperature. In total, the 3D printed ABS-MOF composites that we have produced show that the material blends the most attractive qualities of each component, processibility and selective gas adsorption. Our approach opens the door for further optimization to match the needs of emerging applications, including gas storage, gas filtration, and real-time chemical sensing.

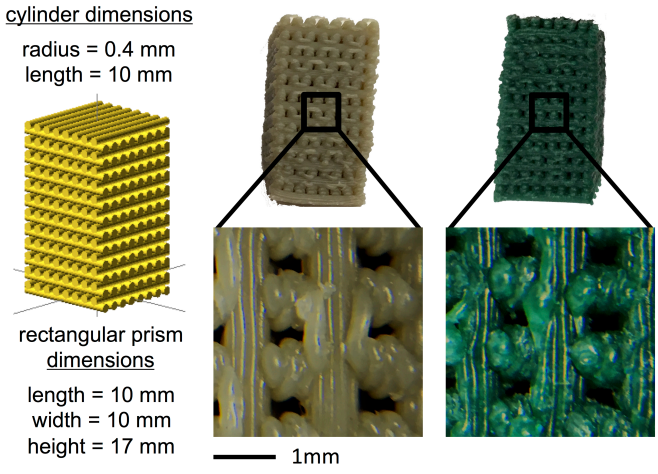

Figure 1. 3D Printed MOF-ABS Composites. The image on the left shows the designed print geometry and dimensions. The image in the middle shows the full printed ABS-ZIF-8 composite (top) and magnified (bottom). The image on the right shows the full printed ABS-HKUST-1 composite (top) and magnified (bottom).

Materials and Methods[25]

1,3,5-benzenetricarboxylic acid (btc) was purchased from TCI. Cupric acetate was purchased from Mallinckrodt. Zinc acetate was purchased from J.T. Baker. 2-methylimidazole and chloroform (HPLC grade, 99.8%) were purchased from Acros Organics. N,N-dimethylformamide (DMF) and triethylamine (TEA) were purchased from EMD Milipore. 200 proof ethanol (EtOH) was purchased from KOPTEC. Dichloromethane was purchased from EMD Millipore. ABS pellets (resin: GPA 100, color #: NC010; color: natural; lot #: C14-0702 K) were acquired from LTL Color Compounders, Inc.

HKUST-1 and ZIF-8 synthesis. HKUST-1 was prepared using a modified literature protocol.[26] btc (4.00 g, 19.04 mmol) was dissolved in 96 mL of a 1:1:1 mixture of DMF:EtOH:H_2O. Cupric acetate (6.88 g, 34.48 mmol) was dissolved in 96 mL of the same solvent mixture. The resulting solutions were combined, stirred, 4 mL of TEA was added, and the mixture continued to stir overnight. To separate the product from the solvent, the mixture was centrifuged (45 minutes at 4000 rpm on a Sorvall RC 6+ centrifuge with an SH-3000 rotor). The supernatant was decanted from the powder, which was then re-dispersed in 40 mL of DMF and centrifuged. The sample was washed in this way an additional 3 times. The product was immersed in 200 mL of dichloromethane overnight. This mixture was centrifuged and washed 3 times with dichloromethane as above. The product was left to sit in 200 mL of dichloromethane overnight. One final centrifugation was performed, the liquid decanted, and the product left to dry in a vacuum oven. The final product was stored in a bell jar containing Drierite.

ZIF-8 was prepared according to literature procedure.[27]

ABS-10% MOF Filament Production. The initial material compounding was performed using a DSM Xplore Micro 15cc Twin Screw Compounder. The compounding temperature was set to 195 °C and the screws turned at 80 rpm. The system was purged with N_2 throughout the compounding process. 12.0 g of ABS pellets were placed into the compounder. The ABS was allowed to melt and mix for 5 minutes after which the extruder head was opened and ABS was extruded. This sample was massed (m_{ABS}) to determine mass of the ABS remaining within the instrument (12.0 –m_{ABS}). A combination of ABS (m_{ABS}-1.2 g) and MOF (1.2 g) was mixed, at the proper ratio, to be compounded with the remaining ABS. This mixture is added to the compounder with the N_2 flow reduced to prevent blowback of the MOF powder. After the first batch of ABS-MOF composite was extruded and weighed ($m_{ABS\text{-}MOF}$), subsequent additions of ABS and MOF to the extruder will be mixtures of 0.9×$m_{ABS\text{-}MOF}$ of ABS and 0.1×$m_{ABS\text{-}MOF}$ of MOF.

To produce a composite filament with the proper diameter for the 3D printer, the compounded composites were first cut into smaller pieces using a wire cutter. These pieces were extruded through a Filabot Wee extruder with a 1.75 mm extrusion nozzle with its temperature set to 195 °C.

Powder X-ray Diffraction. X-ray diffraction (XRD) patterns were recorded using a Rigaku MiniFlex II Desktop X-ray diffractometer equipped with a NaI scintillation counter detector, a 450 W Cu K α (λ=1.540562 Å) X-ray source and a diffracted beam monochromator. The instrument was operated at 30 kV and 15 mA with a scan speed of 5 s/step and a step size of 0.02°. Data was collected for 2θ between 3° and 30°. Discs of the

ABS-MOF composite materials were prepared using a Carver hydraulic press. The press was heated to 195 °C. 1.05 g of the composite was placed in a 2 mm thick, 23 mm diameter circular stainless steel mold. The filled mold, between 2 pieces of Kapton film, was placed into the press and the press was engaged with a force of 5000 metric tons. The disc was left under pressure for 30 minutes after which the heating element was turned off and water-cooled. To test the stability of the MOF within the composite left open to atmosphere, several XRD measurements were taken between 1 and 28 days after compounding. Additionally, the samples were also submerged in water for 1 week after which they were dried and XRD spectra were recorded.

Fourier Transform Infrared (FTIR) Spectroscopy. FTIR spectra were recorded using a Bruker ALPHA FTIR with a diamond head platinum ATR accessory. FTIR spectra were collected as transmission spectra as an average of 24 scans at a resolution of 4 cm^{-1}. ABS-MOF samples were prepared for FTIR spectroscopy using the hydraulic press. A small sample of ABS-MOF was placed between 2 pieces of Kapton film (no molds were used) and pressed using the same protocol as above. These samples resulted in films that were roughly 0.1 mm thick.

Differential Scanning Calorimetry (DSC). DSC measurements were performed using a TA DSC Q2000 Differential Scanning Calorimeter. Heat flow was recorded over the following temperature cycling. The sample was equilibrated at 20.0 °C for 2 minutes followed by a temperature increase to 245.0 °C at a rate of 10.0 °C/min. The temperature was lowered to 20.0 °C at a rate of 10.0 °C/min. This procedure was repeated 2 extra times for each sample. Samples were prepared by weighing roughly 3 mg into a T-zero aluminum pan (TA Instruments) with no lid.

Thermogravimetric Analysis (TGA). TGA measurements were performed using a TA Q500 thermal analysis system with the sample (roughly 5 mg) held in a platinum pan. Samples were recorded in a nitrogen atmosphere. For the measurements, the temperature was increased to 110.0 °C at 10.0 °C/min upon which the temperature was held for 30 minutes. The temperature was then increased to 800.0 °C at 10.0 °C/min.

3D Printing. A Flashforge Creator 3D printer was used to print objects. Any commercial thermoplastic printer could have been used. We have found that the following procedure has given the best results when printing objects with MOF-ABS composites. The printing platform was covered with Kapton film. A 15% (w/v) slurry of ABS suspended in acetone was poured onto this surface, and the acetone was allowed to evaporate during the preheating process. The slurry was the best solution we have found to ensuring that the object does not release from the platform during the printing process. The open faces of the printer were covered with plexiglass (sides) while the top was capped with a box to help maintain a constant internal temperature. With no filament loaded, 30 minute preheat period (platform temperature = 115 °C, nozzle temperature = 220 °C) was performed to minimize internal temperature gradients. The filament was loaded, after which a print job can commence.

The printed geometries (Figure 1) were designed using OpenSCAD software. The program used to generate the geometry is given in the supporting information. The print speed used was 10 mm/s in the x, y, and z directions.

To keep the printer extrusion head as clean as possible, we have found it is best to remove the filament after each print job and floss the extruder opening with piano wire.

Failure to do this results in accumulation of inorganic material within the extruder over time and eventual blockage.

Gas Adsorption: Isotherm at 77 K. Isotherm measurements were performed on a Micrometrics ASAP 2020 Plus accelerated surface-area and porosimetry system. Data analysis was performed using Micromeritics Microactive interactive data reduction software. Analyses were performed at 77 K using N_2 (99.999%). Prior to all adsorption experiments, the samples were degassed for 16 hours under vacuum (1.33 Pa) and at a temperature of 353 K. Sample masses used for these measurements were around 200 mg. Powder samples were used as synthesized. We found that the printed pieces were too thick to allow full gas uptake on the time scales allowed by the instrument parameters. Therefore, polymer and composite samples were prepared as films in the same manner as in the preparation of FTIR samples.

Gas Adsorption and Desorption Kinetics at Room Temperature. All measurements for gas adsorption and desorption were recorded using a previously reported, custom-built apparatus, as described in the supplemental information file. For comparison, the authors previously determined gas adsorption kinetics for 3D printed pure ABS.[28]

Adsorption measurements were carried out as follows. The sample was placed in the sample chamber and degassed by heating to 103 °C for 5 days under vacuum. The nominal mass for the printed ABS-ZIF-8 composite (Figure 1) was 1.1349 g. The nominal mass for the printed ABS-HKUST-1 composite (Figure 1) was 1.1080 g. The sample chamber and reference chamber were initially filled to the same N_2 pressure (roughly 62 kPa). The two chambers were isolated from one another by closing the valve

between them, and the pressure difference between these chambers was measured using a differential capacitance diaphragm gauge.

Desorption measurements were carried out using the same apparatus. The sample was placed in the sample chamber and degassed at 103 °C for 5 days under vacuum. The sample was loaded with N_2 gas at a pressure of roughly 62 kPa for 3-5 days. The sample chamber was isolated from the reference chamber by shutting the valve connecting them. While the reference chamber was continuously evacuated, the pressure rise in the sample chamber was measured using a differential capacitance diaphragm gauge.

Adsorption and desorption rates were fit using double exponential equations with MatLab.

Results and Discussion

One of the primary challenges to realizing the potential of MOFs is their processibility. The powdered forms that most MOFs are synthesized as are difficult to work with. These powders also preclude the materials from reaching the gas storage performance benchmarks that are being defined by the United States Department of Energy.[29] To address these issues, materials scientists have adopted several approaches which include compressing the MOF powders into pellets,[30] developing methodologies for growing ever larger MOF crystals[31] and fabrication of MOF films on pristine surfaces using atomic layer deposition techniques.[32-34]

There has also been a concerted effort to incorporate MOFs into polymers.[19-21] These composite materials include examples where a MOF is incorporated into a polymer, [17,

35] coupled synthesis of polymer and MOF,[36] MOF is synthesized using polymeric materials, [22, 23] and MOFs being grown off of existing polymeric structures.[37]

We modeled our approach for generating ABS-MOF composites on the industrial practice of melt-blend compounding. In this way, the composites we describe can be manufactured on a much larger scale to meet any need for these high-performance materials. As our goal was successful 3D printing of the composites, ABS and PLA were the natural choices due to their ubiquity in 3D printers available to home enthusiasts. The experience and suggestions found online in message boards and other platforms were crucial for helping to optimize our processes. We chose ABS as it has been the easier of the two polymers to compound and form into properly sized filaments for printing. (PLA has a tendency to adsorb water, which in turn leads to polymer and MOF decomposition during compounding and can also lead the production of filaments with too high a variation in their diameter.) For our efforts we have produced ABS-MOF composites that are printable using standard, commercial, thermoplastic 3D printers. Because of the modular nature of our approach, we should be able to optimize our system (polymer, MOF, and printed geometry) as required for different applications.

Structural Properties of ABS-MOF Composites.

We tested for several structural and physical properties of our ABS-MOF composites. Figure 2 shows the powder XRD scattering patterns for each of the MOFs, ABS, and the ABS-MOF composites when exposed to humid environments. Of particular note, in this regard, are the samples that were immersed in water for 7 days. For each recorded sample, the scattering pattern and intensities reflect the composition: ABS shows a broad

scattering that ranges over the full measurement range and the MOF-specific scattering peaks do not change from the powder to the composite.

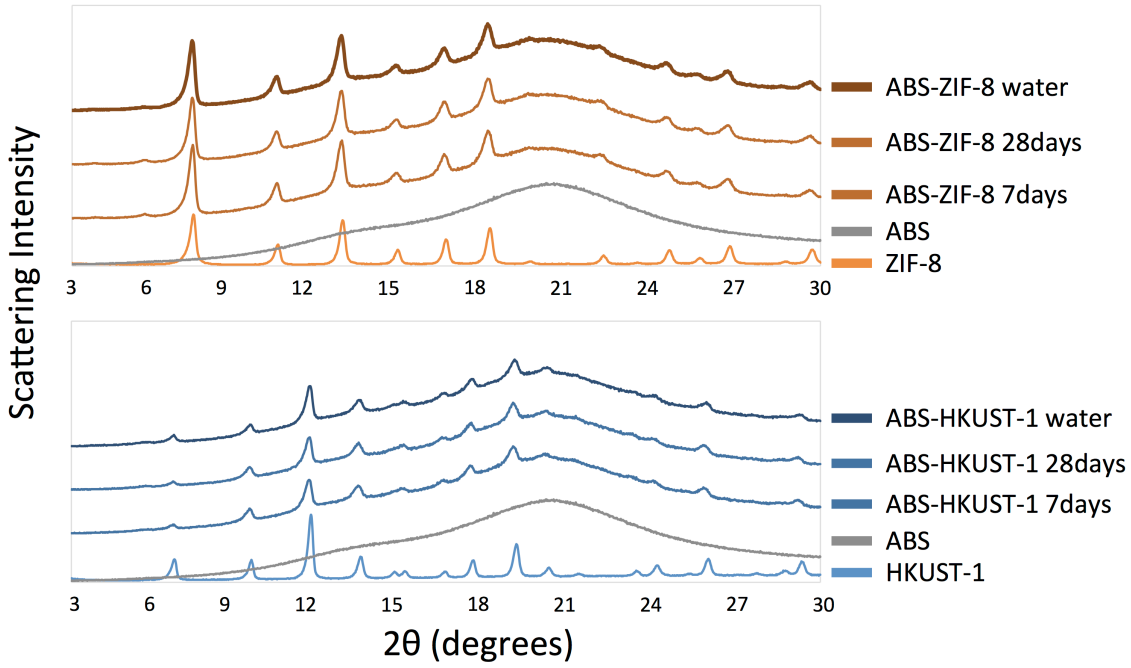

Figure 2. X-ray diffraction scattering patterns. The top panel shows the scattering patterns for ZIF-8, ABS, ABS-ZIF-8 composites exposed to ambient humidity for 7 and 28 days, and ABS-ZIF-8 composite immersed in water for 7 days. The bottom panel shows the scattering patterns for HKUST-1, ABS, ABS-HKUST-1 composites exposed to ambient humidity for 7 and 28 days, and ABS-HKUST-1 composite immersed in water for 7 days.

Powdered HKUST-1 is prone to degradation in humid environments. A previous study has shown that incorporating this MOF into a polymer can increase its stability to water.[17] We have observed a similar effect in our composites. After exposure for 7 and 28 days, the XRD patterns for these samples are not noticeably altered from the linear combination of the HKUST-1 and ABS patterns. Taking this measurement to an extreme, we immersed the composite samples in water for a week. Even after this treatment, there is no noticeable change to the scattering pattern of either MOF within ABS. This result is due to the lower relative humidity within the ABS matrix. We have previously measured

the water uptake at saturation in ABS to be 0.36% by weight when exposed to 57% relative humidity at 22.2 °C;[28] this corresponds to a molar fraction of about 4%. Supporting this observation is another previous experiment where we show that water and aqueous analytes gain access to the interior of a printed ABS-composite structure,[11] the concentration of that water within the polymer is never high enough to cause degradation of the MOF.

The FTIR spectra are shown in Figure 3. (The raw data can be found in the Supporting Information.) Both sets of composite spectra reproduce the features and general intensities expected from a combination of the particular MOF and ABS. This is another indication that the compounding and printing process do not noticeably alter the chemical structure or composition of the polymer or the MOF.

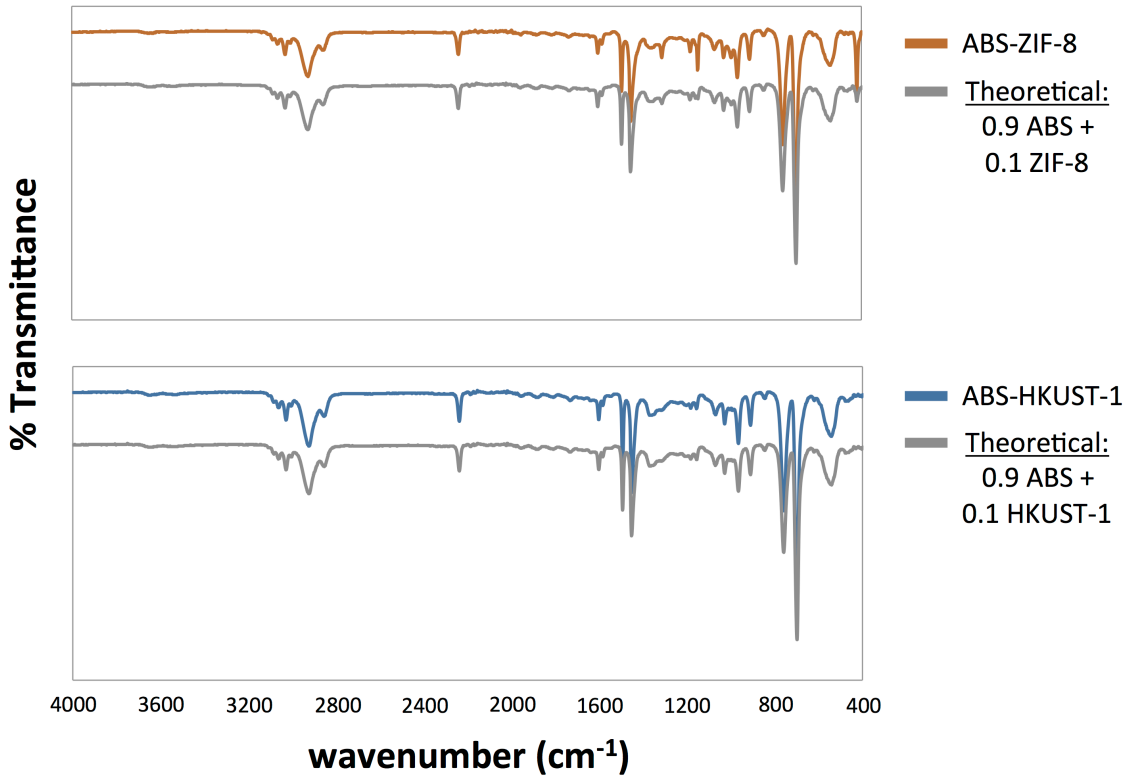

Figure 3. FTIR Spectra of the ABS-MOF composites. The top panel shows the FTIR spectra for ABS-ZIF-8 and a theoretical prediction for the ABS-ZIF-8 spectrum calculated from a linear combination of 0.9(ABS spectrum) and 0.1(ZIF-8 spectrum), reflecting the relative composition of each in the composite. The bottom panel shows the FTIR spectra for ABS-HKUST-1 and a theoretical prediction for the ABS-HKUST-1 spectrum calculated from a linear combination of 0.9(ABS spectrum) and 0.1(HKUST-1 spectrum).

The MOF inserts, however, do have an effect on some of the physical and chemical properties of ABS. TGA measurements (Figure 4) show that both MOFs change the pyrolysis of ABS in similar ways. (The raw data can be found in the Supporting Information.) The ZIF-8 decomposition begins at around 550 °C with the sharpest loss in mass occurring at around 625 °C. The HKUST-1 displays broad loss of mass starting near 200 °C with the primary decomposition occurring near 375 °C. When in the composite, both MOFs decrease the temperature at which the polymer decomposes. Within the composite, HKUST-1 shows some decomposition near 300 °C.

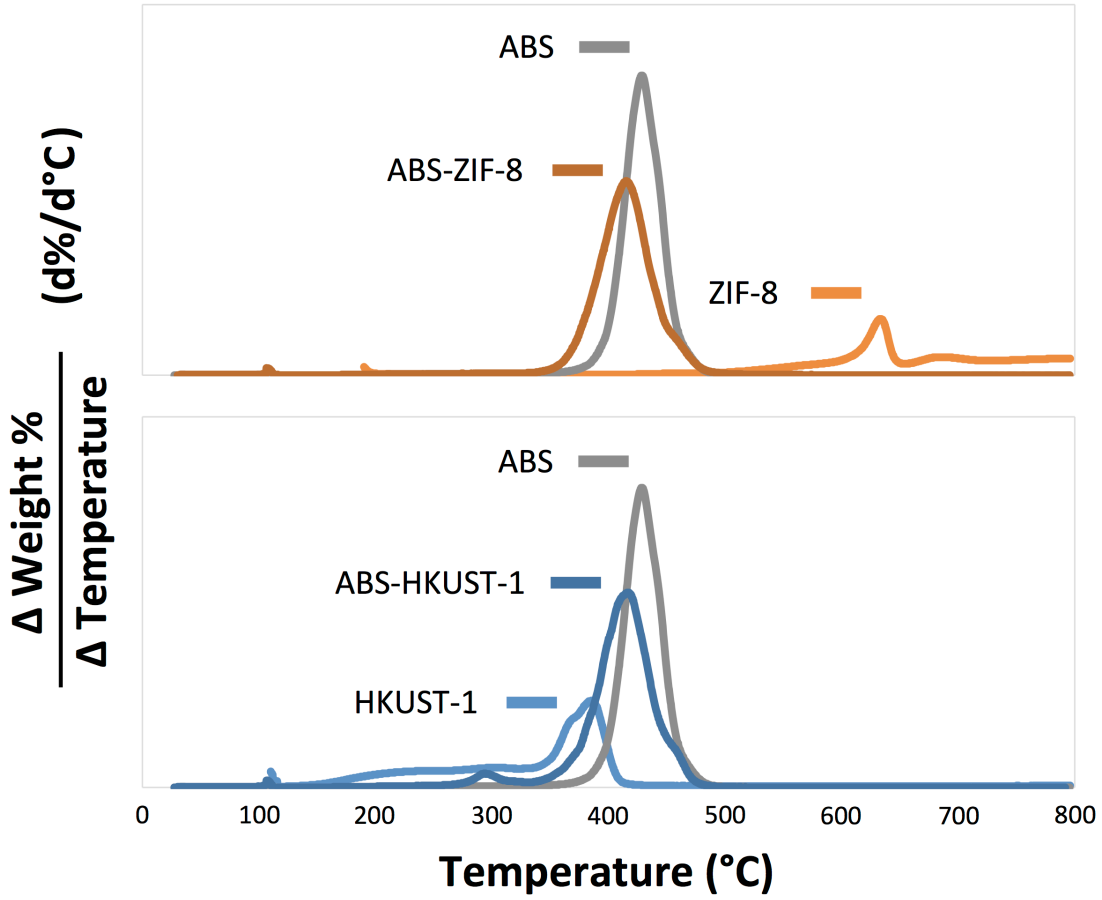

Figure 4. TGA analysis of the ABS-MOF Composites. Both graphs show the first derivative of weight percentage as a function of temperature for all materials under an N_2 atmosphere. The raw data are shown in the supporting information. The top panel shows the data for ABS, ZIF-8, and the ABS-ZIF-8 composite. The bottom panel shows the data for ABS, HKUST-1, and the ABS-HKUST-1 composite.

Importantly, for our studies, the decompositions observed in the composite materials occur at temperatures well above where the materials are 3D printed (220 °C). In processing the materials to make the composites they are heated to 195 °C for 5 minutes (during melt compounding). When 3D printed, the composites are only exposed to the elevated temperature (220 °C) of the print nozzle for a very short period of time (seconds, at most) as the filament is being drawn through the printer head. The TGA data show that the temperatures needed for decomposition exceed the requirements for processing and

printing. The XRD (Figure 2) and FTIR (Figure 3) also show that there is only minor evidence of HKUST-1 decomposition. In general, these data agree with the analysis of the TGA results in that the compounding and printing procedures do not significantly degrade the MOF materials.

DSC measurements (Table 1 – averaged over multiple scans and samples), were also performed to determine how the added MOF affects the properties of the polymer. As expected, the MOFs, on their own, show no thermal transitions within the temperature range studied (20 °C – 245 °C). The glass transition temperature (T_g) of the ABS-ZIF-8 composite is similar to that of pure ABS. The T_g of the ABS-HKUST-1 shows a significant increase over the same transition for pure ABS. While the absolute increase of T_g will not affect the way in which the composite is printed (at 220 °C), the relative increase over the ABS T_g indicates that the individual polymer molecules have stronger interactions with one another. While the polymers themselves, in this case, do not form crystalline structures, HKUST-1 does perturb the polymer structure such that its brittle glassy phase gains stability over its viscous, fluid-like phase. These physical changes have a measured impact on gas adsorption capacity and adsorption and desorption kinetics as shown below.

Table 1. DSC measured glass transition temperatures

Glass Transition Temperature (°C)				
ZIF-8	HKUST-1	ABS	ABS-ZIF-8	ABS-HKUST-1
-	-	104 ± 1	103.7 ± 0.9	106.8 ± 0.6

Gas Adsorption and Adsorption Properties of ABS-MOF Composites

We measured the gas adsorption isotherms (Figure 5) for the MOFs, ABS, and the ABS-MOF composites. The pure MOF's show higher gas adsorption properties than either ABS or the ABS-MOF composites. This is to be expected as the MOFs only make up 10% of the composite material. The ABS-HKUST-1 composite shows a similar adsorption profile to ABS. The ABS-ZIF-8 sample adsorbs significantly more than either of the other two polymer samples.

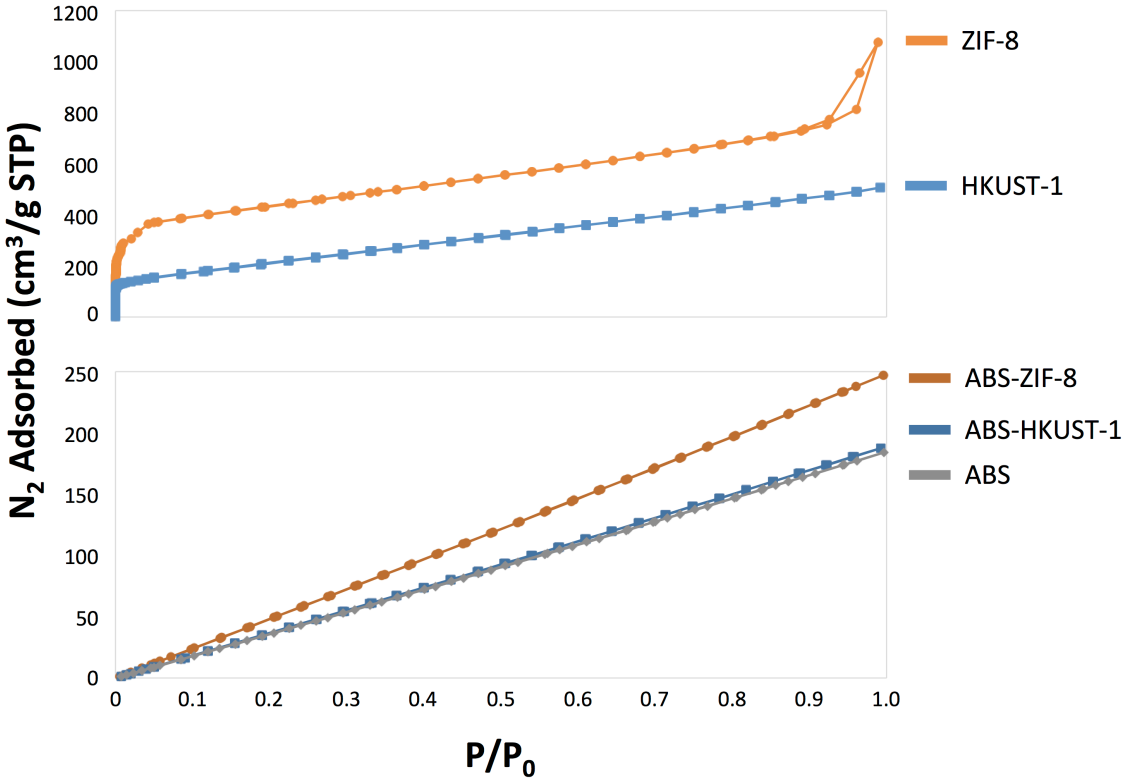

Figure 5. N_2 adsorption isotherms at 77K. The top panel shows the adsorption data for the pure MOF compounds, ZIF-8 and HKUST-1. The bottom panel shows the adsorption data for ABS and the two composites, ABS-ZIF-8 and ABS-HKUST-1.

Of particular note in the N_2-adsorption curves for the ABS-materials is the absence of a dramatic increase in N_2 adsorbed at low relative pressures. For the pure MOF materials,

this rise indicates a microporous structure within the bulk material. We do not observe any microporous structure in the ABS-MOF composites. There are several possibilities for this observation. The microporous structure may be destroyed as a result of the compounding process. This seems unlikely as the X-ray and FTIR data (Figures 2 and 3) correspond to the presence of HKUST-1 and ZIF-8 after compounding. Another possibility includes the prospect that the ABS blocks entry of the gas and prevents it from accessing the interior of the MOF. It does not appear that blocking occurs for the ABS-ZIF-8 sample at higher pressures, though. A final possibility, and one that we find more convincing, is that the slow diffusion through ABS at these low pressures, prevent N2 from accessing all of the microporous states on the time scale of the instrumental measurements. As the pressure increases, there is a larger driving force for the gas to diffuse through the solid, leading to faster access by the gas to the MOF.

We analyzed several adsorption properties (Brunaer-Emmet-Teller (BET) surface area, Horvath-Kawazoe (H-K) maximum pore volume, and quantity adsorbed at $P/P_0 = 0.92$) calculated from these isotherems. These quantities are shown in Table 2. Along with listing the values, we have performed an analysis of the data for the composite material. Specifically, using the data for the pure materials (ABS, ZIF-8, and HKUST-1), we have made estimates of the theoretical predictions for the BET surface area and quantity adsorbed for the composite materials. That is, for example, the ABS-ZIF-8 composite material is composed of 10% ZIF-8 and 90% ABS. The BET surface area and quantity adsorbed for the composite material should be a simple linear combination of 10% of these values for ZIF-8 and 90% of these values for the ABS.

Table 2. Gas adsorption properties of the ABS-MOF composites from the isotherm data

Experimental Values			
Material	BET Surface Area (m^2/g)	H-K Maximum Pore Volume (cm^3/g)	Quantity Adsorbed at $P/P_0 = 0.92$ (cm^3/g STP)
ZIF-8	1446	0.655	753
HKUST-1	776	0.298	476
ABS	332	0.043	169
ABS-ZIF-8	436	0.065	229
ABS-HKUST-1	329	0.044	174
Theoretical ABS-MOF BET Surface Area from Components (m^2/g) [0.9×BET(ABS) + 0.1×BET(MOF)]			
ABS-ZIF-8	435		
ABS-HKUST-1	368		
Theoretical ABS-MOF Quantity Adsorbed from Components (cm^3/g) [0.9×Quantity Adsorbed(ABS) + 0.1×Quantity Adsorbed(MOF)]			
ABS-ZIF-8			227
ABS-HKUST-1			200

Several observations can be made from this analysis. The first is that the ABS-ZIF-8 data are clearly reproduced by their representative components (10% ZIF-8 and 90% ABS). This finding corresponds with our analysis that the microporous structure is missing from these isotherms due to slow diffusion times and not from the absence of the porous MOF structure. This is certainly not the case for the ABS-HKUST-1 data, whose adsorption properties are much lower than is theoretically predicted. From our XRD and FTIR studies, we can rule out degradation or loss of HKUST-1 as being the primary cause. The likely cause of lower gas adsorption in ABS-HKUST-1 composite is structural changes in the polymer that impact gas diffusion/adsorption properties of the composite material. This description is consistent with the DSC observations that indicate tighter polymer packing as evidenced by increased T_g (Table 1). We contend that this characterization of the ABS-HKUST-1 system is supported by the room temperature N_2 uptake analysis presented below.

The N_2 adsorption and desorption kinetics at room temperature (Figure 6) support the analysis of a decreased ABS gas binding capacity in the HKUST-1 composite. For these experiments, the adsorption properties of printed pieces (Figure 1) were measured. For the isotherm data, the printed objects were too thick, presenting too large a barrier to diffusion for the data collection and resulting in gas adsorption capacity values and internal surface area values that were much lower than expected. Using a custom instrument, which measures the pressure differential between two chambers, we measured the N_2 adsorption and desorption by the printed ABS-MOF composites. The mass of the printed pieces for ABS-ZIF-8 and ABS-HKUST-1 were within 0.02 grams of one another (1.135 and 1.108 grams, respectively). The printed ABS-HKUST-1 object adsorbs more N_2 than does the ABS-ZIF-8. This result is consistent with crystallographic evidence that there are more specific gas binding sites within HKUST-1 than ZIF-8.[38]

The gas adsorption and desorption rates are given in Table 3. The slower uptake and release of N_2 by the ABS-HKUST-1 sample also indicates that diffusion through the composite is more hindered than in ABS-ZIF-8, in agreement with our description of altered polymer packing within the ABS-HKUST-1. For both samples, ABS-HKUST-1 and ABS-ZIF-8, the observation that the uptake is faster than the release indicates that there is some attractive interaction between the composite material and N_2. That these rates are different between each composite (HKUST-1 vs ZIF-8) indicates that this attraction is driven by an interaction between N_2 and the MOF as opposed to the N_2 and the ABS. The possibility remains that the compounding process induces new vacancies within the bulk ABS, and these vacancies are what lead to differences in adsorption. However, we contend that the full data set (material analysis in conjunction with N_2

adsorption) argue for the MOF playing an important role in gas uptake in the printed composites.

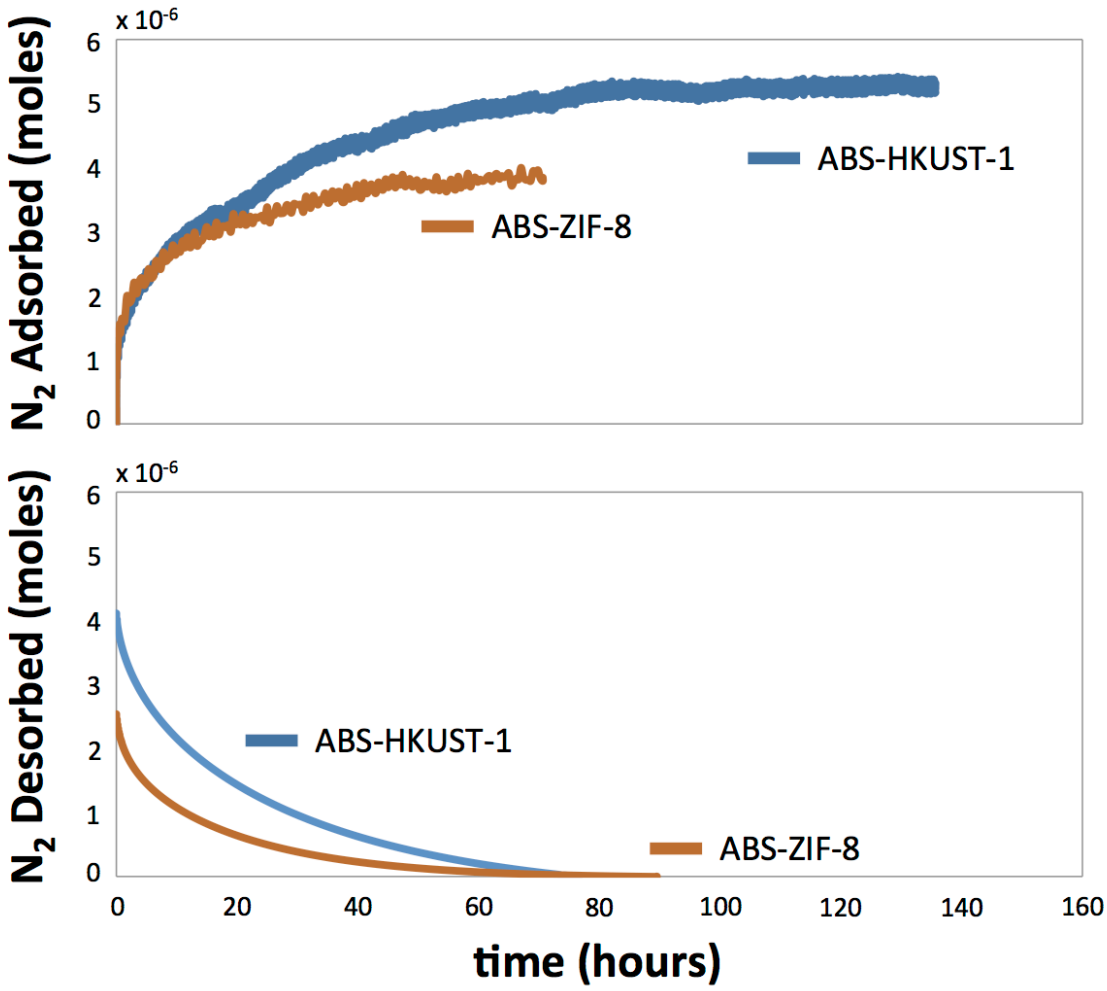

Figure 6. N_2 adsorption and desorption kinetics of ABS-MOF composites at room temperature. The top panel shows the N_2 adsorption of ABS-ZIF-8 and ABS-HKUST-1 as a function of time. The bottom panel shows the N_2 desorption of ABS-ZIF-8 and ABS-HKUST-1 as a function of time. The noise in the adsorption data is higher as the background pressure, from which pressure changes are measured, is higher than is the case for the desorption data.

Table 3. N2 adsorption and desorption rates for the ABS-MOF composites.
$N_2\ adsorbed = a \times exp^{-k_a t} + b \times exp^{-k_b t} - (a+b)$;
$N_2\ desorbed = a + b - a \times exp^{-k_a t} - b \times exp^{-k_b t}$

		$\frac{a}{(a+b)} \times 100$	k_a (h^{-1})	$\frac{b}{(a+b)} \times 100$	k_b (h^{-1})
ABS-HKUST-1	Adsorption	30	3.1	70	0.036
	Desorption	22	0.5	77	0.035
ABS-ZIF-8	Adsorption	45	5.7	55	0.052
	Desorption	29	0.78	71	0.05

Conclusions

MOF-based materials have shown great promise for applications in gas storage, sensing, filtering, and catalysis, among others. One of the primary barriers to realizing their full potential has been processibility. Using the 3D printed ABS-MOF composites we have presented here as a framework, some of these issues can begin to be addressed. Certainly there are some shortcomings to our system as well. Some of these shortcomings can be tailored through material optimization based upon the specific application the user wants to address. In our system, for example, the diffusion barrier resulting from the ABS matrix would be detrimental for use in a gas filtering scheme. Optimizing the system, through a choice of a different polymer would help to remedy that. This is not to say that ABS may not be a useful polymer for any application. We can imagine applications where slow release of adsorbed gases is crucial. As the number of different polymers being used in conventional thermoplastic printers continues to grow, so does the potential for adjustments to our system. Because of the modularity of 3D printing, we have the ability to alter the polymer, MOF, and printed geometry to suit a desired application.

Another shortcoming that we need to address is the low MOF loading percentage. As yet, we are only realizing 10% MOF within our composite. To maximize the ability of our 3D printed objects to interact with gas molecules, it would be advantageous to maximize the content of MOF within the polymer. Our efforts to push past the 10% loading barrier have thus far resulted in filaments that are often too brittle to print. We contend that we will be able to push these boundaries by using plasticizers, functionalizing synthesized MOFs, or borrowing the approach of Cohen to synthesize MOFs using polymeric materials.[22]

As with other 3D printing applications, however, the most enabling aspect of the technology is the ability to achieve complex and functional geometries. We expect that the protocols described within this study will empower the use of material geometries for advanced MOF-based applications.

Acknowledgements

We would like to thank Prof. Douglas Fox of American University for the use of his twin-screw compounder and hydraulic press.

Contact

hartings@american.edu; zeeshan.ahmed@nist.gov

References

[1] M.D. Symes, P.J. Kitson, J. Yan, C.J. Richmond, G.J.T. Cooper, R.W. Bowman, T. Vilbrandt, L. Cronin, Integrated 3D-printed reactionware for chemical synthesis and analysis, Nature Chemistry 4(5) (2012) 349-354.
[2] P.J. Kitson, M.D. Symes, V. Dragone, L. Cronin, Combining 3D printing and liquid handling to produce user-friendly reactionware for chemical synthesis and purification, Chem. Sci. 4(8) (2013) 3099-3103.

[3] C.A. Mandon, L.J. Blum, C.A. Marquette, Adding Biomolecular Recognition Capability to 3D Printed Objects, Anal. Chem. 88(21) (2016) 10767-10772.
[4] M. Guvendiren, J. Molde, R.M.D. Soares, J. Kohn, Designing Biomaterials for 3D Printing, Acs Biomaterials Science & Engineering 2(10) (2016) 1679-1693.
[5] S. Rhee, J.L. Puetzer, B.N. Mason, C.A. Reinhart-King, L.J. Bonassar, 3D Bioprinting of Spatially Heterogeneous Collagen Constructs for Cartilage Tissue Engineering, Acs Biomaterials Science & Engineering 2(10) (2016) 1800-1805.
[6] X.H. Wang, Q. Ao, X.H. Tian, J. Fan, Y.J. Wei, W.J. Hou, H. Tong, S.L. Bai, 3D Bioprinting Technologies for Hard Tissue and Organ Engineering, Materials 9(10) (2016).
[7] M.S. Mannoor, Z. Jiang, T. James, Y.L. Kong, K.A. Malatesta, W.O. Soboyejo, N. Verma, D.H. Gracias, M.C. McAlpine, 3D Printed Bionic Ears, Nano Letters 13(6) (2013) 2634-2639.
[8] B. Duan, L.A. Hockaday, K.H. Kang, J.T. Butcher, 3D Bioprinting of heterogeneous aortic valve conduits with alginate/gelatin hydrogels, Journal of Biomedical Materials Research Part A 101(5) (2013) 1255-1264.
[9] L.A. Hockaday, K.H. Kang, N.W. Colangelo, P.Y.C. Cheung, B. Duan, E. Malone, J. Wu, L.N. Girardi, L.J. Bonassar, H. Lipson, C.C. Chu, J.T. Butcher, Rapid 3D printing of anatomically accurate and mechanically heterogeneous aortic valve hydrogel scaffolds, Biofabrication 4(3) (2012).
[10] J.R. Tumbleston, D. Shirvanyants, N. Ermoshkin, R. Janusziewicz, A.R. Johnson, D. Kelly, K. Chen, R. Pinschmidt, J.P. Rolland, A. Ermoshkin, E.T. Samulski, J.M. DeSimone, Continuous liquid interface production of 3D objects, Science 347(6228) (2015) 1349-1352.
[11] M.R. Skorski, J.M. Esenther, Z. Ahmed, A.E. Miller, M.R. Hartings, The chemical, mechanical, and physical properties of 3D printed materials composed of TiO2-ABS nanocomposites, Sci. Tech. Adv. Mater. 17(1) (2016) 89-97.
[12] C. Zhu, T.Y.J. Han, E.B. Duoss, A.M. Golobic, J.D. Kuntz, C.M. Spadaccini, M.A. Worsley, Highly compressible 3D periodic graphene aerogel microlattices, Nature Communications 6 (2015).
[13] B.L. Chen, S.C. Xiang, G.D. Qian, Metal-Organic Frameworks with Functional Pores for Recognition of Small Molecules, Acc. Chem. Res. 43(8) (2010) 1115-1124.
[14] H. Furukawa, K.E. Cordova, M. O'Keeffe, O.M. Yaghi, The Chemistry and Applications of Metal-Organic Frameworks, Science 341(6149) (2013) 974-+.
[15] J.R. Li, R.J. Kuppler, H.C. Zhou, Selective gas adsorption and separation in metal-organic frameworks, Chem. Soc. Rev. 38(5) (2009) 1477-1504.
[16] S.T. Meek, J.A. Greathouse, M.D. Allendorf, Metal-Organic Frameworks: A Rapidly Growing Class of Versatile Nanoporous Materials, Adv. Mat. 23(2) (2011) 249-267.
[17] J.B. DeCoste, M.S. Denny, G.W. Peterson, J.J. Mahle, S.M. Cohen, Enhanced aging properties of HKUST-1 in hydrophobic mixed-matrix membranes for ammonia adsorption, Chem. Sci. 7(4) (2016) 2711-2716.
[18] Y. Ming, J. Purewal, J. Yang, C.C. Xu, R. Soltis, J. Warner, M. Veenstra, M. Gaab, U. Muller, D.J. Siegel, Kinetic Stability of MOF-5 in Humid Environments: Impact of Powder Densification, Humidity Level, and Exposure Time, Langmuir 31(17) (2015) 4988-4995.

[19] B. Seoane, J. Coronas, I. Gascon, M.E. Benavides, O. Karvan, J. Caro, F. Kapteijn, J. Gascon, Metal-organic framework based mixed matrix membranes: a solution for highly efficient CO2 capture?, Chem. Soc. Rev. 44(8) (2015) 2421-2454.
[20] B. Zornoza, C. Tellez, J. Coronas, J. Gascon, F. Kapteijn, Metal organic framework based mixed matrix membranes: An increasingly important field of research with a large application potential, Micropor. Mesopor. Mat. 166 (2013) 67-78.
[21] Q.L. Zhu, Q. Xu, Metal-organic framework composites, Chem. Soc. Rev. 43(16) (2014) 5468-5512.
[22] Z.J. Zhang, H.T.H. Nguyen, S.A. Miller, S.M. Cohen, polyMOFs: A Class of Interconvertible Polymer-Metal-Organic-Framework Hybrid Materials, Angew. Chem. Int. Edit. 54(21) (2015) 6152-6157.
[23] Z.J. Zhang, H.T.H. Nguyen, S.A. Miller, A.M. Ploskonka, J.B. DeCoste, S.M. Cohen, Polymer-Metal-Organic Frameworks (polyMOFs) as Water Tolerant Materials for Selective Carbon Dioxide Separations, J. Am. Chem. Soc. 138(3) (2016) 920-925.
[24] M.S. Denny, S.M. Cohen, In Situ Modification of Metal-Organic Frameworks in Mixed-Matrix Membranes, Angew. Chem. Int. Edit. 54(31) (2015) 9029-9032.
[25] Certain equipment and materials are identified in this paper in order to specify the experimental procedure adequately. Such identification is not intended to imply endorsement by the National Institute of Standards and Technology, nor is it intended to imply that the materials or equipment identified are necessarily the best available. .
[26] D.J. Tranchemontagne, J.R. Hunt, O.M. Yaghi, Room temperature synthesis of metal-organic frameworks: MOF-5, MOF-74, MOF-177, MOF-199, and IRMOF-0, Tetrahedron 64(36) (2008) 8553-8557.
[27] Y.C. Pan, Y.Y. Liu, G.F. Zeng, L. Zhao, Z.P. Lai, Rapid synthesis of zeolitic imidazolate framework-8 (ZIF-8) nanocrystals in an aqueous system, Chemical Communications 47(7) (2011) 2071-2073.
[28] M. Sefa, Z. Ahmed, J.A. Fedchak, J. Scherschligt, N. Klimov, Gas uptake of 3D printed acrylonitrile butadiene styrene using a vacuum apparatus designed for absorption and desorption studies, Journal of Vacuum Science & Technology A 34(6) (2016).
[29] J.P. Ortmann, N.S. Kaisare, Modeling of cryo-adsorption of hydrogen on MOF-5 pellets: Effect of pellet properties on moderate pressure refueling, International Journal of Hydrogen Energy 41(1) (2016) 342-354.
[30] J.J. Purewal, D. Liu, J. Yang, A. Sudik, D.J. Siegel, S. Maurer, U. Müller, Increased volumetric hydrogen uptake of MOF-5 by powder densification, International Journal of Hydrogen Energy 37(3) (2012) 2723-2727.
[31] L.N. Li, F.X. Sun, J.T. Jia, T. Borjigin, G.S. Zhu, Growth of large single MOF crystals and effective separation of organic dyes, Crystengcomm 15(20) (2013) 4094-4098.
[32] L.C. Gallington, I.S. Kim, W.-G. Liu, A.A. Yakovenko, A.E. Platero-Prats, Z. Li, T.C. Wang, J.T. Hupp, O.K. Farha, D.G. Truhlar, A.B.F. Martinson, K.W. Chapman, Regioselective Atomic Layer Deposition in Metal–Organic Frameworks Directed by Dispersion Interactions, J. Am. Chem. Soc. 138(41) (2016) 13513-13516.
[33] J.E. Mondloch, W. Bury, D. Fairen-Jimenez, S. Kwon, E.J. DeMarco, M.H. Weston, A.A. Sarjeant, S.T. Nguyen, P.C. Stair, R.Q. Snurr, O.K. Farha, J.T. Hupp, Vapor-Phase

Metalation by Atomic Layer Deposition in a Metal-Organic Framework, J. Am. Chem. Soc. 135(28) (2013) 10294-10297.
[34] K. Leus, J. Dendooven, N. Tahir, R.K. Ramachandran, M. Meledina, S. Turner, G. Van Tendeloo, J.L. Goeman, J. Van der Eycken, C. Detavernier, P. Van Der Voort, Atomic Layer Deposition of Pt Nanoparticles within the Cages of MIL-101: A Mild and Recyclable Hydrogenation Catalyst, Nanomaterials 6(3) (2016).
[35] L.D. O'Neill, H.F. Zhang, D. Bradshaw, Macro-/microporous MOF composite beads, Journal of Materials Chemistry 20(27) (2010) 5720-5726.
[36] C.L. Calvez, M. Zouboulaki, C. Petit, L. Peeva, N. Shirshova, One step synthesis of MOF-polymer composites, RSC Advances 6(21) (2016) 17314-17317.
[37] Z. Wang, J. Wang, M. Li, K. Sun, C.-j. Liu, Three-dimensional Printed Acrylonitrile Butadiene Styrene Framework Coated with Cu-BTC Metal-organic Frameworks for the Removal of Methylene Blue, Sci. Rep. 4 (2014) 5939.
[38] E.J. Carrington, I.J. Vitórica-Yrezábal, L. Brammer, Crystallographic studies of gas sorption in metal–organic frameworks, Acta Crystallographica Section B, Structural Science, Crystal Engineering and Materials 70(Pt 3) (2014) 404-422.

Supporting Information for:
3D printed ABS-MOF composite materials and their gas storage properties

Michael Bible[a], Makfir Sefa[b], James A. Fedchak[b], Julia Scherschligt[b], Zeeshan Ahmed[b]*, Matthew R. Hartings[a]*

[a]Department of Chemistry, American University, 4400 Massachusetts Ave., NW, Washington, DC 20016, USA

[b]Thermodynamic Metrology Group, Sensor Science Division, Physical Measurement Laboratory, National Institute of Standards and Technology, Gaithersburg, MD 20899, USA

I. Room temperature gas adsorption and desorption

Below is an example for how the gas absorption and desorption measurements were carried out.

Background (Empty chamber)

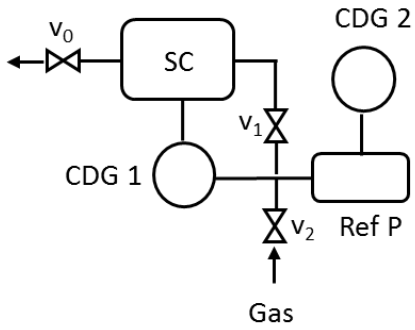

CDG 1- Differential gauge (1 Torr), CDG 2 Capacitance diaphragm gauge (1000 Torr), Ref P – reference pressure and v_0, $v_1$and v_2 –Valves.

- System was baked for 5 days at 150 ^{0}C then cooled to room temperature
- Filled **Ref P** chamber with nitrogen gas through valve V_2 at pressure P=126 kPa then V_2 was closed, valve V_1 was closed, and V_0 was opened.
- V_1 was opened, while keeping V_0 and V_2 were closed; therefore N_2 expanded into SC and the total pressure fell to P=55 kPa. Valve V_1 was closed after 60 s.

- The differential pressure change ΔP (CDG 1) and reference pressure P_{Ref} (CDG2) were logged for 70 h

  Pressure in the SC was calculated as:

$$P_{SC} = \Delta P + P_{Ref} \qquad (1)$$

  Where ΔP is differential pressure was measured with CDG1 and P_{Refa} reference pressure was measured with CDG 2.

  Pressure P_{sc} is converted to moles using the ideal gas law:

$$\Delta n = \frac{P_{SC} V_{SC}}{RT} \qquad (2)$$

  V_{SC} volume of the SC chamber V_{SC} = 0.2 L, the gas constant R = 8314 Pa L mol^{-1} K^{-1} and T= 295.2 K was the gas temperature

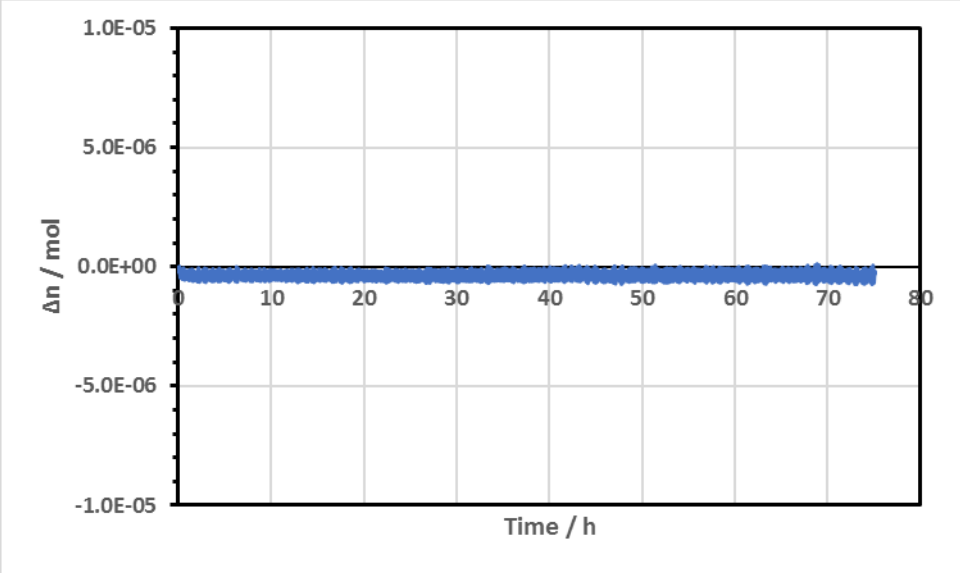

Figure S2. N_2 absorption measurement of empty chamber

N_2 absorption on 3D printed ABS-ZIF-8

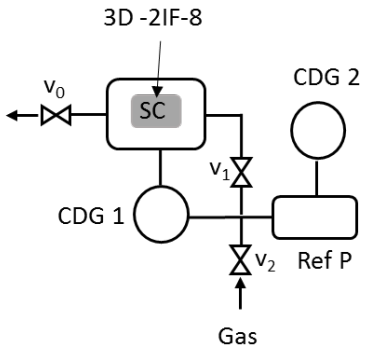

CDG 1- Differential gauge (1 Torr), CDG 2 Capacitance diaphragm gauge (1000 Torr), Ref P – reference pressure and v_0, $v_1$and v_2 –Valves.

- Place 3D printed ABS-ZIF-8 in the SC
- System was baked for 5 days at 103 ^{0}C.
- The same procedure was repeated as in the background measurement (above)

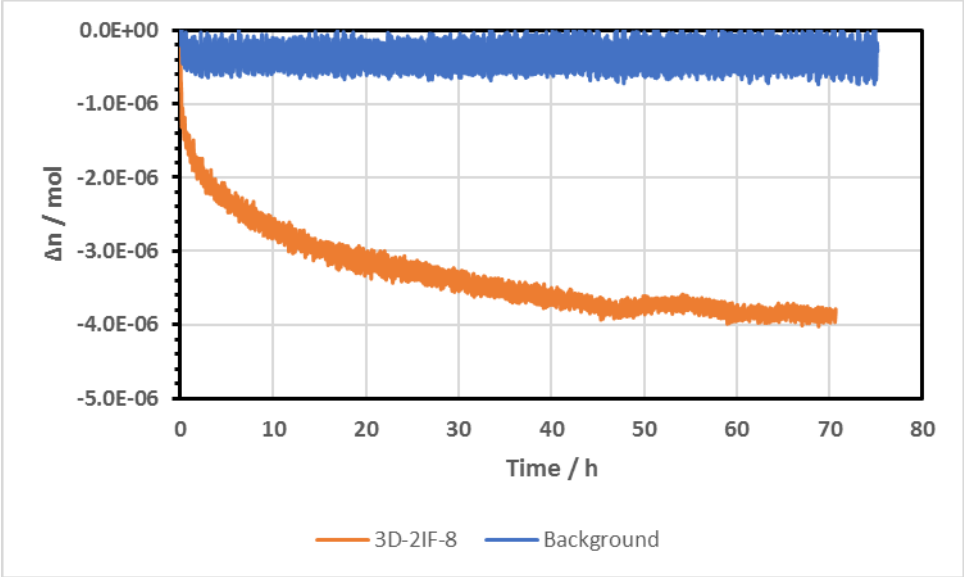

Figure S3. N_2 absorption measurement of empty chamber (Blue) and chamber with 3D printed ABS-ZIF-8 sample previously degassed in vacuum for 5 days at 100 °C (Orange)

****

N_2 desorption from 3D printed ABS-ZIF-8

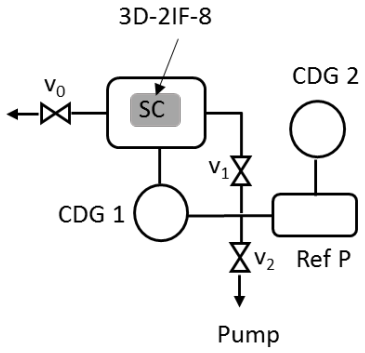

CDG 1- Differential gauge (1 Torr), CDG 2 Capacitance diaphragm gauge (1000 Torr), Ref P – reference pressure and v_0, $v_1$and v_2 –Valves.

- ABS-ZIF-8 was exposed to P nitrogen for 70 hours while valves V_0, V_1 and V_2 were closed
- With V_0 closed, valves V_2 and V_1 were opened to evacuate nitrogen from **SC** and **Ref** chamber. Valve V_1 was re-closed after 4 minutes.
- Pressure change in the SC was measured with CDG 1.
- Pressure rise P_{sc} is converted to moles using the ideal gas law

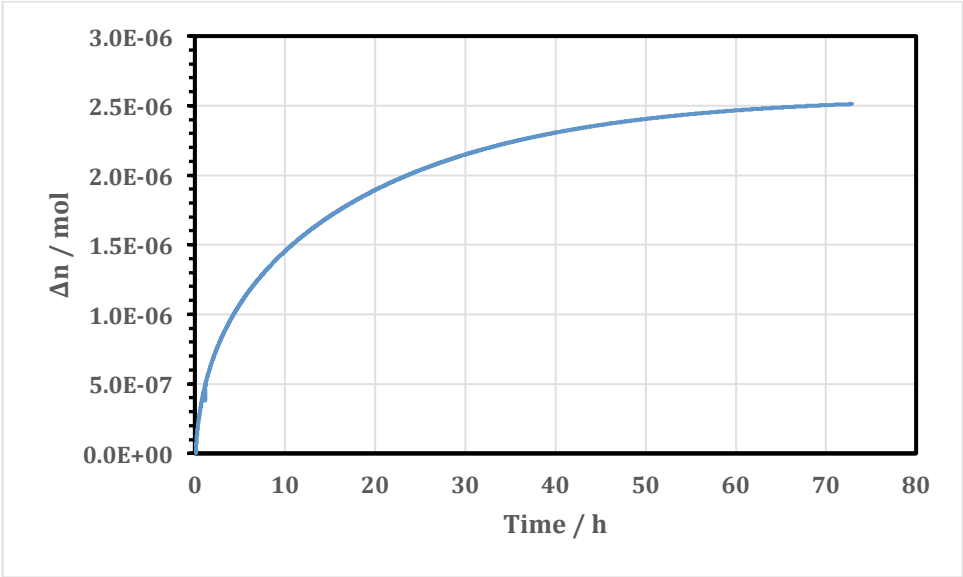

Figure S4. N_2 desorption measurement of chamber with 3D printed ABS-ZIF-8 sample previously exposed to nitrogen for 70 h

III. Thermogravimentric analysis data

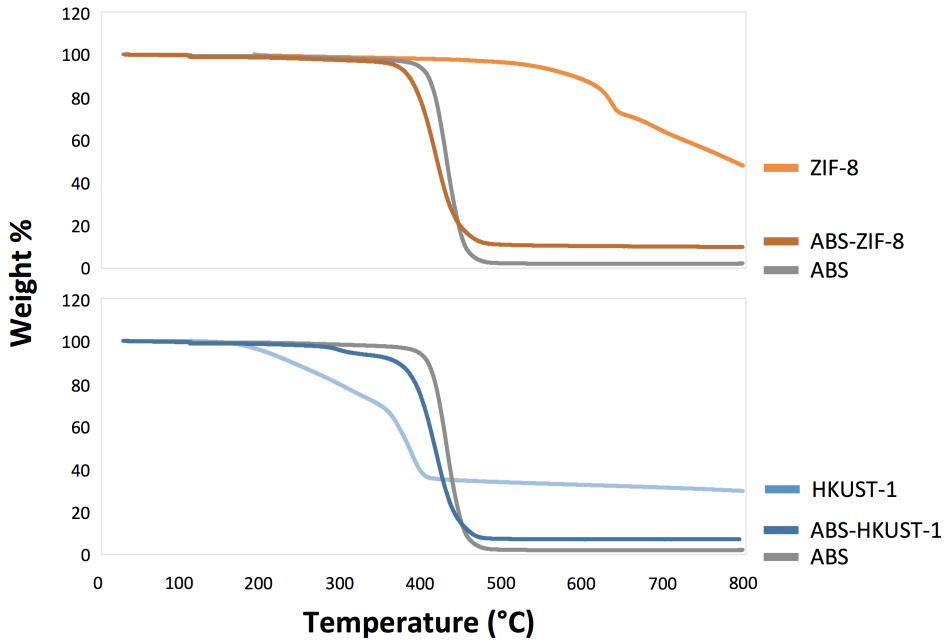

Figure S5. Thermogravimetric data for ABS-MOF composites.

III. FTIR data

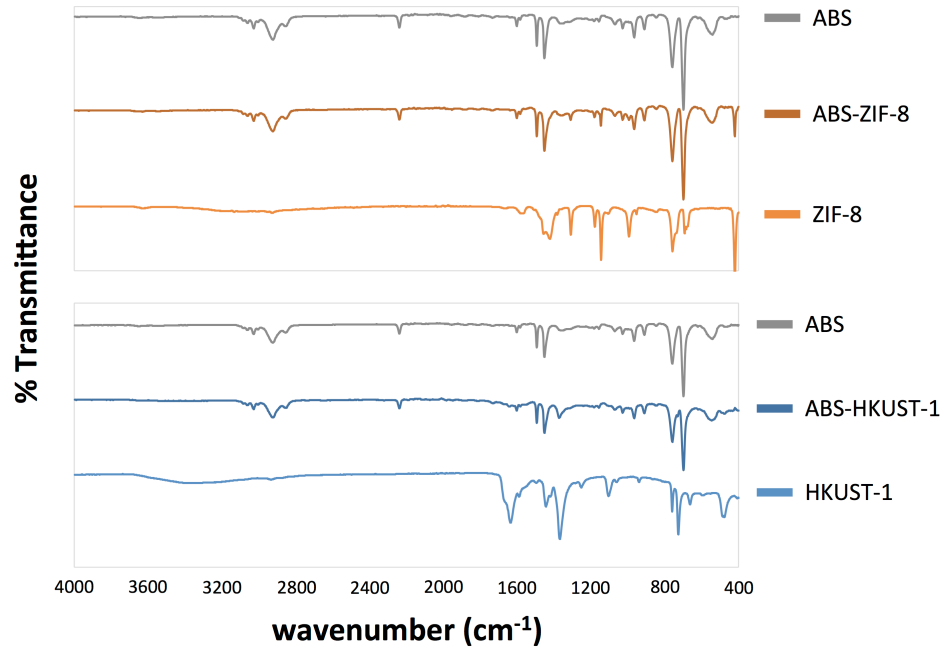

Figure S6. FTIR data for ABS-MOF composites.

III. OpenSCAD file used to generate printed geometry

```
{
rotate ([90,0,0])
translate([4.2,0,-5])
cylinder(r=0.4,h=10,$fn=20) ;

rotate ([90,0,0])
translate([3,0,-5])
cylinder(r=0.4,h=10,$fn=20) ;

rotate ([90,0,0])
translate([1.8,0,-5])
cylinder(r=0.4,h=10,$fn=20) ;

rotate ([90,0,0])
translate([0.6,0,-5])
cylinder(r=0.4,h=10,$fn=20) ;

rotate ([90,0,0])
translate([-0.6,0,-5])
cylinder(r=0.4,h=10,$fn=20) ;

rotate ([90,0,0])
translate([-1.8,0,-5])
cylinder(r=0.4,h=10,$fn=20) ;

rotate ([90,0,0])
translate([-3,0,-5])
cylinder(r=0.4,h=10,$fn=20) ;

rotate ([90,0,0])
translate([-4.2,0,-5])
cylinder(r=0.4,h=10,$fn=20) ;

rotate ([0,90,0])
translate([-0.7,4.2,-5])
cylinder(r=0.4,h=10,$fn=20) ;

rotate ([0,90,0])
translate([-0.7,3,-5])
cylinder(r=0.4,h=10,$fn=20) ;

rotate ([0,90,0])
translate([-0.7,1.8,-5])
cylinder(r=0.4,h=10,$fn=20) ;
```

```
rotate ([0,90,0])
translate([-0.7,0.6,-5])
cylinder(r=0.4,h=10,$fn=20) ;

rotate ([0,90,0])
translate([-0.7,-0.6,-5])
cylinder(r=0.4,h=10,$fn=20) ;

rotate ([0,90,0])
translate([-0.7,-1.8,-5])
cylinder(r=0.4,h=10,$fn=20) ;

rotate ([0,90,0])
translate([-0.7,-3,-5])
cylinder(r=0.4,h=10,$fn=20) ;

rotate ([0,90,0])
translate([-0.7,-4.2,-5])
cylinder(r=0.4,h=10,$fn=20) ;

rotate ([90,0,0])
translate([4.2,1.4,-5])
cylinder(r=0.4,h=10,$fn=20) ;

rotate ([90,0,0])
translate([3,1.4,-5])
cylinder(r=0.4,h=10,$fn=20) ;

rotate ([90,0,0])
translate([1.8,1.4,-5])
cylinder(r=0.4,h=10,$fn=20) ;

rotate ([90,0,0])
translate([0.6,1.4,-5])
cylinder(r=0.4,h=10,$fn=20) ;

rotate ([90,0,0])
translate([-0.6,1.4,-5])
cylinder(r=0.4,h=10,$fn=20) ;

rotate ([90,0,0])
translate([-1.8,1.4,-5])
cylinder(r=0.4,h=10,$fn=20) ;

rotate ([90,0,0])
```

```
translate([-3,1.4,-5])
cylinder(r=0.4,h=10,$fn=20) ;

rotate ([90,0,0])
translate([-4.2,1.4,-5])
cylinder(r=0.4,h=10,$fn=20) ;

rotate ([0,90,0])
translate([-2.1,4.2,-5])
cylinder(r=0.4,h=10,$fn=20) ;

rotate ([0,90,0])
translate([-2.1,3,-5])
cylinder(r=0.4,h=10,$fn=20) ;

rotate ([0,90,0])
translate([-2.1,1.8,-5])
cylinder(r=0.4,h=10,$fn=20) ;

rotate ([0,90,0])
translate([-2.1,0.6,-5])
cylinder(r=0.4,h=10,$fn=20) ;

rotate ([0,90,0])
translate([-2.1,-0.6,-5])
cylinder(r=0.4,h=10,$fn=20) ;

rotate ([0,90,0])
translate([-2.1,-1.8,-5])
cylinder(r=0.4,h=10,$fn=20) ;

rotate ([0,90,0])
translate([-2.1,-3,-5])
cylinder(r=0.4,h=10,$fn=20) ;

rotate ([0,90,0])
translate([-2.1,-4.2,-5])
cylinder(r=0.4,h=10,$fn=20) ;

rotate ([90,0,0])
translate([4.2,2.8,-5])
cylinder(r=0.4,h=10,$fn=20) ;

rotate ([90,0,0])
translate([3,2.8,-5])
cylinder(r=0.4,h=10,$fn=20) ;
```

```
rotate ([90,0,0])
translate([1.8,2.8,-5])
cylinder(r=0.4,h=10,$fn=20) ;

rotate ([90,0,0])
translate([0.6,2.8,-5])
cylinder(r=0.4,h=10,$fn=20) ;

rotate ([90,0,0])
translate([-0.6,2.8,-5])
cylinder(r=0.4,h=10,$fn=20) ;

rotate ([90,0,0])
translate([-1.8,2.8,-5])
cylinder(r=0.4,h=10,$fn=20) ;

rotate ([90,0,0])
translate([-3,2.8,-5])
cylinder(r=0.4,h=10,$fn=20) ;

rotate ([90,0,0])
translate([-4.2,2.8,-5])
cylinder(r=0.4,h=10,$fn=20) ;

rotate ([0,90,0])
translate([-3.5,4.2,-5])
cylinder(r=0.4,h=10,$fn=20) ;

rotate ([0,90,0])
translate([-3.5,3,-5])
cylinder(r=0.4,h=10,$fn=20) ;

rotate ([0,90,0])
translate([-3.5,1.8,-5])
cylinder(r=0.4,h=10,$fn=20) ;

rotate ([0,90,0])
translate([-3.5,0.6,-5])
cylinder(r=0.4,h=10,$fn=20) ;

rotate ([0,90,0])
translate([-3.5,-0.6,-5])
cylinder(r=0.4,h=10,$fn=20) ;

rotate ([0,90,0])
```

```
translate([-3.5,-1.8,-5])
cylinder(r=0.4,h=10,$fn=20) ;

rotate ([0,90,0])
translate([-3.5,-3,-5])
cylinder(r=0.4,h=10,$fn=20) ;

rotate ([0,90,0])
translate([-3.5,-4.2,-5])
cylinder(r=0.4,h=10,$fn=20) ;

rotate ([90,0,0])
translate([4.2,4.2,-5])
cylinder(r=0.4,h=10,$fn=20) ;

rotate ([90,0,0])
translate([3,4.2,-5])
cylinder(r=0.4,h=10,$fn=20) ;

rotate ([90,0,0])
translate([1.8,4.2,-5])
cylinder(r=0.4,h=10,$fn=20) ;

rotate ([90,0,0])
translate([0.6,4.2,-5])
cylinder(r=0.4,h=10,$fn=20) ;

rotate ([90,0,0])
translate([-0.6,4.2,-5])
cylinder(r=0.4,h=10,$fn=20) ;

rotate ([90,0,0])
translate([-1.8,4.2,-5])
cylinder(r=0.4,h=10,$fn=20) ;

rotate ([90,0,0])
translate([-3,4.2,-5])
cylinder(r=0.4,h=10,$fn=20) ;

rotate ([90,0,0])
translate([-4.2,4.2,-5])
cylinder(r=0.4,h=10,$fn=20) ;

rotate ([0,90,0])
translate([-4.9,4.2,-5])
cylinder(r=0.4,h=10,$fn=20) ;
```

```
rotate ([0,90,0])
translate([-4.9,3,-5])
cylinder(r=0.4,h=10,$fn=20) ;

rotate ([0,90,0])
translate([-4.9,1.8,-5])
cylinder(r=0.4,h=10,$fn=20) ;

rotate ([0,90,0])
translate([-4.9,0.6,-5])
cylinder(r=0.4,h=10,$fn=20) ;

rotate ([0,90,0])
translate([-4.9,-0.6,-5])
cylinder(r=0.4,h=10,$fn=20) ;

rotate ([0,90,0])
translate([-4.9,-1.8,-5])
cylinder(r=0.4,h=10,$fn=20) ;

rotate ([0,90,0])
translate([-4.9,-3,-5])
cylinder(r=0.4,h=10,$fn=20) ;

rotate ([0,90,0])
translate([-4.9,-4.2,-5])
cylinder(r=0.4,h=10,$fn=20) ;

rotate ([90,0,0])
translate([4.2,5.6,-5])
cylinder(r=0.4,h=10,$fn=20) ;

rotate ([90,0,0])
translate([3,5.6,-5])
cylinder(r=0.4,h=10,$fn=20) ;

rotate ([90,0,0])
translate([1.8,5.6,-5])
cylinder(r=0.4,h=10,$fn=20) ;

rotate ([90,0,0])
translate([0.6,5.6,-5])
cylinder(r=0.4,h=10,$fn=20) ;

rotate ([90,0,0])
```

```
translate([-0.6,5.6,-5])
cylinder(r=0.4,h=10,$fn=20) ;

rotate ([90,0,0])
translate([-1.8,5.6,-5])
cylinder(r=0.4,h=10,$fn=20) ;

rotate ([90,0,0])
translate([-3,5.6,-5])
cylinder(r=0.4,h=10,$fn=20) ;

rotate ([90,0,0])
translate([-4.2,5.6,-5])
cylinder(r=0.4,h=10,$fn=20) ;

rotate ([0,90,0])
translate([-6.3,4.2,-5])
cylinder(r=0.4,h=10,$fn=20) ;

rotate ([0,90,0])
translate([-6.3,3,-5])
cylinder(r=0.4,h=10,$fn=20) ;

rotate ([0,90,0])
translate([-6.3,1.8,-5])
cylinder(r=0.4,h=10,$fn=20) ;

rotate ([0,90,0])
translate([-6.3,0.6,-5])
cylinder(r=0.4,h=10,$fn=20) ;

rotate ([0,90,0])
translate([-6.3,-0.6,-5])
cylinder(r=0.4,h=10,$fn=20) ;

rotate ([0,90,0])
translate([-6.3,-1.8,-5])
cylinder(r=0.4,h=10,$fn=20) ;

rotate ([0,90,0])
translate([-6.3,-3,-5])
cylinder(r=0.4,h=10,$fn=20) ;

rotate ([0,90,0])
translate([-6.3,-4.2,-5])
cylinder(r=0.4,h=10,$fn=20) ;
```

```
rotate ([90,0,0])
translate([4.2,7,-5])
cylinder(r=0.4,h=10,$fn=20) ;

rotate ([90,0,0])
translate([3,7,-5])
cylinder(r=0.4,h=10,$fn=20) ;

rotate ([90,0,0])
translate([1.8,7,-5])
cylinder(r=0.4,h=10,$fn=20) ;

rotate ([90,0,0])
translate([0.6,7,-5])
cylinder(r=0.4,h=10,$fn=20) ;

rotate ([90,0,0])
translate([-0.6,7,-5])
cylinder(r=0.4,h=10,$fn=20) ;

rotate ([90,0,0])
translate([-1.8,7,-5])
cylinder(r=0.4,h=10,$fn=20) ;

rotate ([90,0,0])
translate([-3,7,-5])
cylinder(r=0.4,h=10,$fn=20) ;

rotate ([90,0,0])
translate([-4.2,7,-5])
cylinder(r=0.4,h=10,$fn=20) ;

rotate ([0,90,0])
translate([-7.7,4.2,-5])
cylinder(r=0.4,h=10,$fn=20) ;

rotate ([0,90,0])
translate([-7.7,3,-5])
cylinder(r=0.4,h=10,$fn=20) ;

rotate ([0,90,0])
translate([-7.7,1.8,-5])
cylinder(r=0.4,h=10,$fn=20) ;

rotate ([0,90,0])
```

```
translate([-7.7,0.6,-5])
cylinder(r=0.4,h=10,$fn=20) ;

rotate ([0,90,0])
translate([-7.7,-0.6,-5])
cylinder(r=0.4,h=10,$fn=20) ;

rotate ([0,90,0])
translate([-7.7,-1.8,-5])
cylinder(r=0.4,h=10,$fn=20) ;

rotate ([0,90,0])
translate([-7.7,-3,-5])
cylinder(r=0.4,h=10,$fn=20) ;

rotate ([0,90,0])
translate([-7.7,-4.2,-5])
cylinder(r=0.4,h=10,$fn=20) ;

rotate ([90,0,0])
translate([4.2,8.4,-5])
cylinder(r=0.4,h=10,$fn=20) ;

rotate ([90,0,0])
translate([3,8.4,-5])
cylinder(r=0.4,h=10,$fn=20) ;

rotate ([90,0,0])
translate([1.8,8.4,-5])
cylinder(r=0.4,h=10,$fn=20) ;

rotate ([90,0,0])
translate([0.6,8.4,-5])
cylinder(r=0.4,h=10,$fn=20) ;

rotate ([90,0,0])
translate([-0.6,8.4,-5])
cylinder(r=0.4,h=10,$fn=20) ;

rotate ([90,0,0])
translate([-1.8,8.4,-5])
cylinder(r=0.4,h=10,$fn=20) ;

rotate ([90,0,0])
translate([-3,8.4,-5])
cylinder(r=0.4,h=10,$fn=20) ;
```

```
rotate ([90,0,0])
translate([-4.2,8.4,-5])
cylinder(r=0.4,h=10,$fn=20) ;

rotate ([0,90,0])
translate([-9.1,4.2,-5])
cylinder(r=0.4,h=10,$fn=20) ;

rotate ([0,90,0])
translate([-9.1,3,-5])
cylinder(r=0.4,h=10,$fn=20) ;

rotate ([0,90,0])
translate([-9.1,1.8,-5])
cylinder(r=0.4,h=10,$fn=20) ;

rotate ([0,90,0])
translate([-9.1,0.6,-5])
cylinder(r=0.4,h=10,$fn=20) ;

rotate ([0,90,0])
translate([-9.1,-0.6,-5])
cylinder(r=0.4,h=10,$fn=20) ;

rotate ([0,90,0])
translate([-9.1,-1.8,-5])
cylinder(r=0.4,h=10,$fn=20) ;

rotate ([0,90,0])
translate([-9.1,-3,-5])
cylinder(r=0.4,h=10,$fn=20) ;

rotate ([0,90,0])
translate([-9.1,-4.2,-5])
cylinder(r=0.4,h=10,$fn=20) ;

rotate ([90,0,0])
translate([4.2,9.8,-5])
cylinder(r=0.4,h=10,$fn=20) ;

rotate ([90,0,0])
translate([3,9.8,-5])
cylinder(r=0.4,h=10,$fn=20) ;

rotate ([90,0,0])
```

```
translate([1.8,9.8,-5])
cylinder(r=0.4,h=10,$fn=20) ;

rotate ([90,0,0])
translate([0.6,9.8,-5])
cylinder(r=0.4,h=10,$fn=20) ;

rotate ([90,0,0])
translate([-0.6,9.8,-5])
cylinder(r=0.4,h=10,$fn=20) ;

rotate ([90,0,0])
translate([-1.8,9.8,-5])
cylinder(r=0.4,h=10,$fn=20) ;

rotate ([90,0,0])
translate([-3,9.8,-5])
cylinder(r=0.4,h=10,$fn=20) ;

rotate ([90,0,0])
translate([-4.2,9.8,-5])
cylinder(r=0.4,h=10,$fn=20) ;

rotate ([0,90,0])
translate([-10.5,4.2,-5])
cylinder(r=0.4,h=10,$fn=20) ;

rotate ([0,90,0])
translate([-10.5,3,-5])
cylinder(r=0.4,h=10,$fn=20) ;

rotate ([0,90,0])
translate([-10.5,1.8,-5])
cylinder(r=0.4,h=10,$fn=20) ;

rotate ([0,90,0])
translate([-10.5,0.6,-5])
cylinder(r=0.4,h=10,$fn=20) ;

rotate ([0,90,0])
translate([-10.5,-0.6,-5])
cylinder(r=0.4,h=10,$fn=20) ;

rotate ([0,90,0])
translate([-10.5,-1.8,-5])
cylinder(r=0.4,h=10,$fn=20) ;
```

```
rotate ([0,90,0])
translate([-10.5,-3,-5])
cylinder(r=0.4,h=10,$fn=20) ;

rotate ([0,90,0])
translate([-10.5,-4.2,-5])
cylinder(r=0.4,h=10,$fn=20) ;

rotate ([90,0,0])
translate([4.2,11.2,-5])
cylinder(r=0.4,h=10,$fn=20) ;

rotate ([90,0,0])
translate([3,11.2,-5])
cylinder(r=0.4,h=10,$fn=20) ;

rotate ([90,0,0])
translate([1.8,11.2,-5])
cylinder(r=0.4,h=10,$fn=20) ;

rotate ([90,0,0])
translate([0.6,11.2,-5])
cylinder(r=0.4,h=10,$fn=20) ;

rotate ([90,0,0])
translate([-0.6,11.2,-5])
cylinder(r=0.4,h=10,$fn=20) ;

rotate ([90,0,0])
translate([-1.8,11.2,-5])
cylinder(r=0.4,h=10,$fn=20) ;

rotate ([90,0,0])
translate([-3,11.2,-5])
cylinder(r=0.4,h=10,$fn=20) ;

rotate ([90,0,0])
translate([-4.2,11.2,-5])
cylinder(r=0.4,h=10,$fn=20) ;

rotate ([0,90,0])
translate([-11.9,4.2,-5])
cylinder(r=0.4,h=10,$fn=20) ;

rotate ([0,90,0])
```

```
translate([-11.9,3,-5])
cylinder(r=0.4,h=10,$fn=20) ;

rotate ([0,90,0])
translate([-11.9,1.8,-5])
cylinder(r=0.4,h=10,$fn=20) ;

rotate ([0,90,0])
translate([-11.9,0.6,-5])
cylinder(r=0.4,h=10,$fn=20) ;

rotate ([0,90,0])
translate([-11.9,-0.6,-5])
cylinder(r=0.4,h=10,$fn=20) ;

rotate ([0,90,0])
translate([-11.9,-1.8,-5])
cylinder(r=0.4,h=10,$fn=20) ;

rotate ([0,90,0])
translate([-11.9,-3,-5])
cylinder(r=0.4,h=10,$fn=20) ;

rotate ([0,90,0])
translate([-11.9,-4.2,-5])
cylinder(r=0.4,h=10,$fn=20) ;

rotate ([90,0,0])
translate([4.2,12.6,-5])
cylinder(r=0.4,h=10,$fn=20) ;

rotate ([90,0,0])
translate([3,12.6,-5])
cylinder(r=0.4,h=10,$fn=20) ;

rotate ([90,0,0])
translate([1.8,12.6,-5])
cylinder(r=0.4,h=10,$fn=20) ;

rotate ([90,0,0])
translate([0.6,12.6,-5])
cylinder(r=0.4,h=10,$fn=20) ;

rotate ([90,0,0])
translate([-0.6,12.6,-5])
cylinder(r=0.4,h=10,$fn=20) ;
```

```
rotate ([90,0,0])
translate([-1.8,12.6,-5])
cylinder(r=0.4,h=10,$fn=20) ;

rotate ([90,0,0])
translate([-3,12.6,-5])
cylinder(r=0.4,h=10,$fn=20) ;

rotate ([90,0,0])
translate([-4.2,12.6,-5])
cylinder(r=0.4,h=10,$fn=20) ;

rotate ([0,90,0])
translate([-13.3,4.2,-5])
cylinder(r=0.4,h=10,$fn=20) ;

rotate ([0,90,0])
translate([-13.3,3,-5])
cylinder(r=0.4,h=10,$fn=20) ;

rotate ([0,90,0])
translate([-13.3,1.8,-5])
cylinder(r=0.4,h=10,$fn=20) ;

rotate ([0,90,0])
translate([-13.3,0.6,-5])
cylinder(r=0.4,h=10,$fn=20) ;

rotate ([0,90,0])
translate([-13.3,-0.6,-5])
cylinder(r=0.4,h=10,$fn=20) ;

rotate ([0,90,0])
translate([-13.3,-1.8,-5])
cylinder(r=0.4,h=10,$fn=20) ;

rotate ([0,90,0])
translate([-13.3,-3,-5])
cylinder(r=0.4,h=10,$fn=20) ;

rotate ([0,90,0])
translate([-13.3,-4.2,-5])
cylinder(r=0.4,h=10,$fn=20) ;

rotate ([90,0,0])
```

```
translate([4.2,14,-5])
cylinder(r=0.4,h=10,$fn=20) ;

rotate ([90,0,0])
translate([3,14,-5])
cylinder(r=0.4,h=10,$fn=20) ;

rotate ([90,0,0])
translate([1.8,14,-5])
cylinder(r=0.4,h=10,$fn=20) ;

rotate ([90,0,0])
translate([0.6,14,-5])
cylinder(r=0.4,h=10,$fn=20) ;

rotate ([90,0,0])
translate([-0.6,14,-5])
cylinder(r=0.4,h=10,$fn=20) ;

rotate ([90,0,0])
translate([-1.8,14,-5])
cylinder(r=0.4,h=10,$fn=20) ;

rotate ([90,0,0])
translate([-3,14,-5])
cylinder(r=0.4,h=10,$fn=20) ;

rotate ([90,0,0])
translate([-4.2,14,-5])
cylinder(r=0.4,h=10,$fn=20) ;

rotate ([0,90,0])
translate([-14.7,4.2,-5])
cylinder(r=0.4,h=10,$fn=20) ;

rotate ([0,90,0])
translate([-14.7,3,-5])
cylinder(r=0.4,h=10,$fn=20) ;

rotate ([0,90,0])
translate([-14.7,1.8,-5])
cylinder(r=0.4,h=10,$fn=20) ;

rotate ([0,90,0])
translate([-14.7,0.6,-5])
cylinder(r=0.4,h=10,$fn=20) ;
```

```
rotate ([0,90,0])
translate([-14.7,-0.6,-5])
cylinder(r=0.4,h=10,$fn=20) ;

rotate ([0,90,0])
translate([-14.7,-1.8,-5])
cylinder(r=0.4,h=10,$fn=20) ;

rotate ([0,90,0])
translate([-14.7,-3,-5])
cylinder(r=0.4,h=10,$fn=20) ;

rotate ([0,90,0])
translate([-14.7,-4.2,-5])
cylinder(r=0.4,h=10,$fn=20) ;

rotate ([90,0,0])
translate([4.2,15.4,-5])
cylinder(r=0.4,h=10,$fn=20) ;

rotate ([90,0,0])
translate([3,15.4,-5])
cylinder(r=0.4,h=10,$fn=20) ;

rotate ([90,0,0])
translate([1.8,15.4,-5])
cylinder(r=0.4,h=10,$fn=20) ;

rotate ([90,0,0])
translate([0.6,15.4,-5])
cylinder(r=0.4,h=10,$fn=20) ;

rotate ([90,0,0])
translate([-0.6,15.4,-5])
cylinder(r=0.4,h=10,$fn=20) ;

rotate ([90,0,0])
translate([-1.8,15.4,-5])
cylinder(r=0.4,h=10,$fn=20) ;

rotate ([90,0,0])
translate([-3,15.4,-5])
cylinder(r=0.4,h=10,$fn=20) ;

rotate ([90,0,0])
```

```
translate([-4.2,15.4,-5])
cylinder(r=0.4,h=10,$fn=20) ;

rotate ([0,90,0])
translate([-16.1,4.2,-5])
cylinder(r=0.4,h=10,$fn=20) ;

rotate ([0,90,0])
translate([-16.1,3,-5])
cylinder(r=0.4,h=10,$fn=20) ;

rotate ([0,90,0])
translate([-16.1,1.8,-5])
cylinder(r=0.4,h=10,$fn=20) ;

rotate ([0,90,0])
translate([-16.1,0.6,-5])
cylinder(r=0.4,h=10,$fn=20) ;

rotate ([0,90,0])
translate([-16.1,-0.6,-5])
cylinder(r=0.4,h=10,$fn=20) ;

rotate ([0,90,0])
translate([-16.1,-1.8,-5])
cylinder(r=0.4,h=10,$fn=20) ;

rotate ([0,90,0])
translate([-16.1,-3,-5])
cylinder(r=0.4,h=10,$fn=20) ;

rotate ([0,90,0])
translate([-16.1,-4.2,-5])
cylinder(r=0.4,h=10,$fn=20) ;
}
```